Optik 126 (2015) 5047–5051

Contents lists available at ScienceDirect

Optik

journal homepage: www.elsevier.de/ijleo

A phase-diversity speckle experimental system for one meter-scale ground-based telescope

Shixue Zhang*, Bin Wang

Changchun Institute of Optics, Fine Mechanics and Physics, Chinese Academy of Sciences, Dongnanhu Road No. 3888, Changchun 130033, China

ARTICLE INFO

Article history:
Received 14 October 2014
Accepted 8 September 2015

Keywords:
Phase diverse speckle
Wave-front aberration
Image restoration
Phase estimation

ABSTRACT

Phase-diversity (PD) is the least square adaptive-filter of the imaging system based on wave optics theory. It can use unknown extended object as the observation object to collect two or more images whose wave-front diversities are known and fixed. According to the images, the wave-front of the optical system can be calculated by PD, and simultaneously the estimation of ideal image for the observation object can be obtained. Phase-diverse speckle (PDS) technique extends PD by using a series of short-expose frames as the input. In this paper, we designed PDS experiment on a 1.23 m telescope and successfully got clear restored images of space objects. Under the observation condition that the atmospheric coherent length was not more than 8 cm at 500 nm wavelength in Changchun city, we replaced the deformable mirror with a plane mirror in adaptive optical system and separately used the moon and Polaris as the observation objects. For Polaris, the FWHW reduced from 20.6 to 5.3 (in pixel), which decreased about 74%. The experimental results demonstrate that PDS algorithm can be used on one meter-scale telescope in practical observation.

1. Introduction

The wave-front phase aberration caused by atmospheric turbulence becomes serious, when the aperture of the ground-base telescope becomes larger [1–7], and that obviously degrades images. The conventional method to solve the above problem is to use Hartmann wave-front detector to detect wave-front information by adaptive optics and calibrate the wave-front by deformable mirror. However, for one meter-scale telescope, D/r_0 is less than 20, and the influence of atmospheric turbulence is much smaller than two meter-scale telescope. The proportion of the adaptive optics system in the total cost is very high, and the maintenance is very expensive, so it is hard to calibrate extended object by adaptive optics system. Therefore it is necessary to find a reliable, low cost method to solve the problem.

Phase-diverse speckle (PDS) is an image restoration method to correct wave-front phase distortion. It combines the advantages of Phase Diversity and speckle imaging, and can not only estimate wave-front phase but also use multiple channels [8]. The structure of PDS optical system is simple, clear and low cost, suitable for both point source objects and extended objects. Besides, PDS has a good performance in image restoration, and it can also be applied to the field of optical detection. It can detect the aberration, alignment errors, mirror flatness and other parameters of the optical system, which provides new ideas and methods for optical detection without suitable collimators [9]. So PDS technique is an important direction to overcome the wave-front phase distortion at present, and it has many irreplaceable advantages.

PD technique was first proposed by Gonsalves in 1979, it extracts phase information from focused and defocused images and recovers the object with known defocus amount. PD technique not only can simplify the optical path of wave-front sensor, but also can detect the wave-front information of the extended object. And it gets rid of the dependence on the point object for a majority of wave-front sensors. Paxman et al. [10–12] further improved PD theory, they proposed PDS technique by collecting one pair or more pairs of short-expose images on focus plane and defocus plane of the imaging system, and gave the mathematical models under Gaussian noise and Poisson noise, which greatly improved the estimation precision. Vogel et al. [13,14] proposed the fast numerical solution by theories about inverse problem. Löfdahl et al. [15,16] successfully applied PDS theory to the field of solar observation and obtained high resolution images of the structure of solar surface. Denolle et al. [17] proposed a new analytical WFS technique that can measure disturbances from the images in a wide range of cases, with various levels of complexity. Blanc et al. [18] proposed a novel method called marginal estimator for estimating the

* Corresponding author. Tel.: +86 431 86708872; fax: +86 431 84627071.
E-mail address: zhangsx@ciomp.ac.cn (S. Zhang).

http://dx.doi.org/10.1016/j.ijleo.2015.09.054
0030-4026/

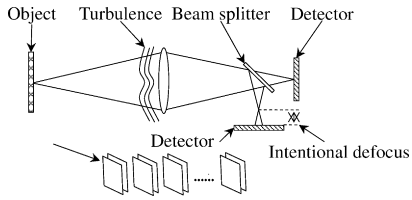

Fig. 1. The scheme of data-collection image by PD.

aberrations and the object from phase-diversity data, and got good results.

Based on the study above, we built PD optical path in the optical box on a 1.23 m telescope without adaptive optical path. Under the observation condition that the atmospheric coherent length was not more than 8 cm at 500 nm wavelength, we separately used the single star, binary star, the moon, Polaris and rocket debris as the observation objects to make the image restoration experiments through PD and got good performance. The experimental results demonstrate the feasibility of using PD in image restoration on one meter-scale telescope without adaptive optical system.

2. Basic principle

It is known that both the process of image restoration and the solution of the wave-front from a single image are ill-posed. The reason is that point-spread function (PSF) can be mapped to multiple wave-fronts. In phase diversity, the incoming wave-front is estimated from at least two images of the same object recorded in presence of a known optical aberration (e.g. defocus), both the unknown incoming wavefront and the observed object can be derived. Phase diversity has the particularity of providing the estimation of the unaberrated object as well as the aberrations responsible for the blurring. This method directly uses image data for the estimation of the aberrations. It is thus sensitive to all aberrations degrading the quality of the imaging telescope, contrarily to WFSs such as the Shack–Hartman, which use a dedicated light path and thus are affected by non-common path aberrations. Furthermore, the optical hardware of PD is simple. Phase diversity is becoming a widespread method both to compensate quasi-static optical aberrations and to obtain diffraction-limited imaging through turbulence.

Fig. 1 illustrates the optical path of PD system. There are focus and defocus collection channels, and the numbers of collection channels can be increased if necessary. The problem of PD image restoration can be regarded as the inverse problem of seeking phase of original signal through the known analog of interference signal or be seen as an adaptive filter.

2.1. Imaging system model

Atmosphere and telescope can be seen as a linear space-invariant system approximately. Under the non-coherent light illumination, the imaging function of Gaussian noise model [1] is

$$d(x) = f(x) * s(x) + n(x) \tag{1}$$

where d is the image of object collected on CCD; f is the ideal image of object; s is the point spread function; n is the Gaussian noise; x is the coordinate of image plane.

In near field, the point spread function [1] is

$$s(x) = \left| \mathcal{F}^{-1} \left\{ P(\upsilon) e^{i\phi(\upsilon)} \right\} \right|^2 \tag{2}$$

where $\mathcal{F}^{-1}$ is Fourier transform; υ are coordinates of the pupil plane; P is the pupil function; ϕ is the wave-front phase, which can be decomposed into a set of Zernike polynomials as

$$\phi(\upsilon) = \theta(\upsilon) + \sum_{m=4}^{M} \alpha_m Z_m(\upsilon) \tag{3}$$

where α_m is the mth coefficient of polynomials; Z_m is the mth base of Zernike polynomials; θ is the known fixed-defocus phase that can be described by

$$\theta(\upsilon) = \frac{2\pi}{\lambda} \frac{z\left(\upsilon_x^2 + \upsilon_y^2\right)}{8(F\#)^2} \tag{4}$$

where υ_x and υ_y are the normalized vectors in pupil plane; z is defocus length; λ is wavelength; $F\#$ is F number.

2.2. Evaluation function

The mathematical model of PD can be regarded as an adaptive filter. In the Gaussian noise model, the mean square deviation of object and multi-channel images can be used as likelihood function. In frequency domain, the evaluation function is

$$L(f, \{\alpha\}_t) = \frac{1}{2N} \sum_u \left(\sum_{t=1}^{T} \sum_{c=1}^{C} \left| D_{tc}(u) - FS_{tc}(u) \right|^2 + \gamma \left| F(u) \right|^2 \right) \tag{5}$$

where u is frequency domain coordinate; T is the number of frames; C is the number of channels, for example, in this paper we use two cameras, so $T = 2$; N is the total number of pixels of the single image; α is the Zernike coefficient needing to be solved; $\mathcal{F}$ is Fourier transform, $D_{tc} = \mathcal{F}(d_{tc})$, $F = \mathcal{F}(f)$, $S_{tc} = \mathcal{F}(s_{tc})$; the second part of the right bracket is Tikhonov regularization term [13,14], which can improve the stability and convergence rate of the algorithm; γ is regular non-negative coefficient.

According to maximum likelihood estimation, target estimation can be regarded as an independent intermediate process and is separated from phase estimation, so we can get the evaluation function unrelated to the target [11]. The expression of target estimation is an intermediate process of derivation of evaluation function. It has the same form as wiener filter and can reduce the effect of noise efficiently.

$$L(\{\alpha\}_t) = \frac{1}{2N} \sum_u \left(\sum_{t=1}^{T} \sum_{c=1}^{C} \left| D_{tc} \right|^2 - \frac{\left| \sum_{t=1}^{T} \sum_{c=1}^{C} D_{tc} S_{tc}^* \right|^2}{\gamma + \sum_{t=1}^{T} \sum_{c=1}^{C} \left| S_{tc} \right|^2} \right) \tag{6}$$

$$F = \frac{\sum_{t=1}^{T} \sum_{c=1}^{C} D_{tc} S_{tc}^*}{\gamma + \sum_{t=1}^{T} \sum_{c=1}^{C} \left| S_{tc} \right|^2} \tag{7}$$

When evaluation function is determined, the process of wave-front detection and image restoration can be described as a mathematical optimization problem. We use the L-BFGS-B algorithm [19–21] which is suitable for large optimization problems and write optimization software by C++ language. After a long-term test, we demonstrate that the algorithm has good convergence efficiency.

3. Experimental design

3.1. Experimental system components

We make the experiment on a 1.23 m telescope, and the system diagram is shown in Fig. 2. The whole optical path is in a metal box which is fixed on the telescope. In order to validate the ability of

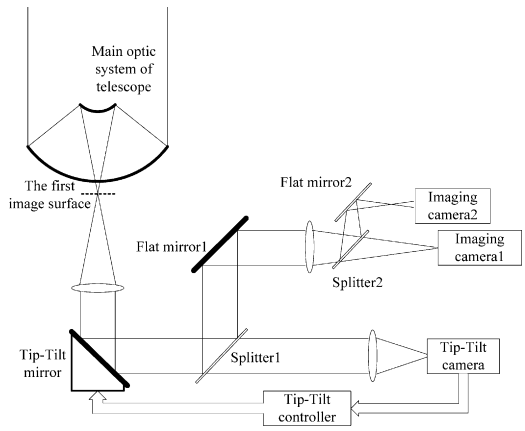

Fig. 2. Structure of experimental system.

Fig. 3. Experimental layout.

image restoration to space objects by PD under atmospheric turbulence, we replaced plane mirror with deformable mirror on the position of Flat mirror1. Therefore, on the whole acquisition process of PD, there was not adaptive optical system to calibrate the aberration caused by atmospheric turbulence.

The difference between the optical paths of PD and normal imaging system is as follows. For PD optical path, it needs at least one designated defocus amount acquisition channel and short exposure, so that the wave-front information will be in the collected images, and the focus plane acquisition channel is synchronous acquisition through external trigger. So it needs to add a spectroscope and a plane mirror behind the imaging lens on the original optical path as shown in Fig. 2. The optical path is divided into two parts, one image on focus plane camera and the other image on defocus plane camera with known defocus amount. In order to keep the relative defocus amount of the two cameras invariant, they are placed on the same electric translation platform as shown in Fig. 3.

The two cameras should be the same scientific CCD cameras and we collect two images on focus plane and defocus plane by synchronous acquisition through external trigger. If the two cameras are not the same type, the pixel size of the two cameras should be the same at least. In our experiment, we use the same camera of Andor897, and its pixel size is 16 μm.

3.2. Experimental system analysis

During the experiment, there were two main problems. The first one is about the alignment of the two cameras, and the second one is the inconsistent readout noise of the two cameras.

For the first problem, compared with using single camera to collect different defocus amount images in different time, the use of two cameras will introduce a new alignment error for PDS and there will be an image rotation between phase surfaces of the two cameras. As the wave-front distortion will not cause image rotation, it is difficult to analyze the effect of designation angle image rotation to the solution of wave-front. So we have to solve this error before PD calculation. There are mainly two steps in our solution. First, during the alignment stage, the shield which had been drilled with several holes was used as the object board, and according to the unshoot amount of the holes on images we readjusted the camera until the relative image rotation of the camera edge was less than 1 pixel. In the second step, we preprocessed the collected images, and made geometric rotation and gray difference transformation. The operations in the first step ensured the relative small image rotation, and only at that time gray difference transformation has high precision [22,23].

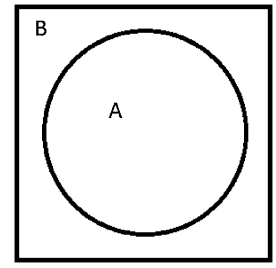

Fig. 4. Spectrum component.

For the second problem, based on the work in reference [10], we involve the variance value of the readout noise in each image, and we can get the objective function of each image with different noise.

$$L(\{\alpha\}_t) = \frac{1}{2N}\sum_u \left(\sum_{t=1}^{T}\sum_{c=1}^{C} \sigma_{tc}^{-2}\left|D_{tc}\right|^2 - \frac{\left|\sum_{t=1}^{T}\sum_{c=1}^{C}\sigma_{tc}^{-2}D_{tc}S_{tc}^*\right|^2}{\gamma + \sum_{t=1}^{T}\sum_{c=1}^{C}\sigma_{tc}^{-2}\left|S_{tc}\right|^2} \right) \quad (8)$$

$$F = \frac{\sum_{t=1}^{T}\sum_{c=1}^{C}\sigma_{tc}^{-2}D_{tc}S_{tc}^*}{\gamma + \sum_{t=1}^{T}\sum_{c=1}^{C}\sigma_{tc}^{-2}\left|S_{tc}\right|^2} \quad (9)$$

where σ_{tc}^{-2} is the reciprocal value of noise variance in frame t, channel c. Eq. (8) is the spectrum of the objective image when the noises of each acquired image are inconsistent. Then we can obtain derivative and gradient of L:

$$\frac{\partial L}{\partial \alpha_m} = \frac{-2}{N}\sum_{x,y\in\chi} \mathcal{Z}_n(x,y)Imag\left(\sum_{c=1}^{C} V_{tc}\right) \quad (10)$$

$$V_{tc} = \sigma_c^{-2}H_{tc}^*\mathcal{F}\left(h_{tc}\mathrm{Real}\left[\mathcal{F}^{-1}\left(F^*D_{tc} - \left|F\right|^2 S_{tc}\right)\right]\right) \quad (11)$$

Then we should estimate the value of σ_{tc}^{-2}. According to Eq. (1) and Fourier transformation feature, we can get

$$D_{tc}(u) = F(u)S_{tc}(u) + N_{tc}(u) \quad (12)$$

Assuming the size of acquired image is $N \times N$, after the Fourier transformation and the movement of frame 0 to the center, its spectrum is as Fig. 1 shows, which is composed of A and B. In Fig. 4, the border line of area A and B are the limiting frequency of the ideal optical system.

So Eq. (9) can be transformed to

$$D_{tc}(u) = \begin{cases} F(u)S_{tc}(u) + N_{tc}(u) & u \in A \\ N_{tc}(u) & u \in B \end{cases} \quad (13)$$

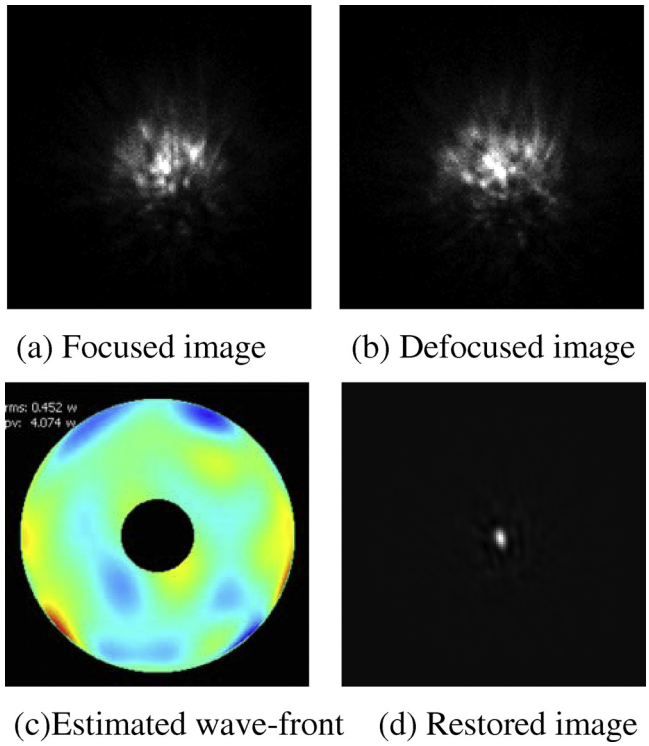

Fig. 5. Original images and result of Polaris.

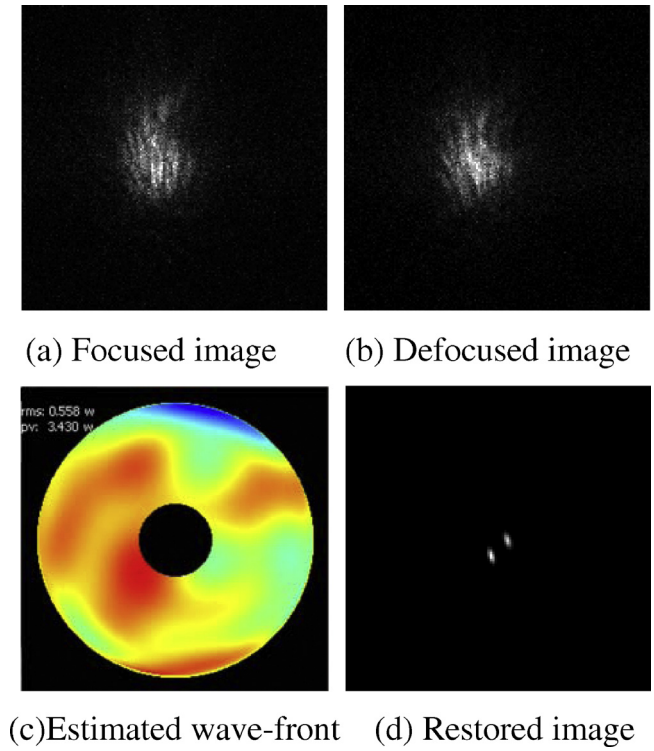

Fig. 6. Original images and results of moon surface.

We assume the noise of each acquired image is independent, and it is Gauss white noise: $n_{tc}(x) \sim N(0, \sigma_{tc}^2)$. So we can get the estimation of σ_{tc}^2:

$$\hat{\sigma}_{tc}^2 = \frac{\sum_u^{u \in B} \left| D_{tc}(u) \right|^2}{N * N * \sum_u^{u \in B} I(u)} \tag{14}$$

where

$$I(u) = \begin{cases} 1 & u \in B \\ 0 & \text{others} \end{cases} \tag{15}$$

It is to be pointed that this estimation method of σ_{tc}^2 is only suitable to the imaging system where camera's acquire frequency is higher than Nyquist frequency, otherwise B is empty set.

4. Experimental results

In our experiment system, the *F#* of imaging camera is 40; the center wavelength is 800 nm; the depth of focus is 2.56 mm. The defocus amount should be selected between 4 to 6 times of the depth of focus, and we selected 11 mm as the defocus amount of defocus channel. The pixel size of the camera is 16 μm. Compared to the previous indoor experiment [24,25], we have made outdoor experiment in Changchun city, and the observed time was during end of August, the atmospheric coherent length was not more than 8 cm at 500 nm wavelength. The exposure time is less than or equal to the atmospheric coherence time.

The observation objects of this experiment were Polaris, and the moon surface. The exposure time is from 5 ms to 10 ms, and the focus and defocus cameras collected images simultaneously by external trigger signals.

First, we used Polaris as the observation object for quantitative analysis of our PDS imaging system.

For the Polaris, we used eight pairs of images as the input. As shown in Fig. 5, (a) and (b) are the focused and the defocused images, and they were collected at the same time. After PDS calculation, we got the estimated wave-front as shown in (c), and the restored image in (d). In image (a) the FWHM is 20.6 (in pixel), while the FWHM in image (d) is 5.3 (in pixel), so the FWHM decreased about 74%.

In order to verify the imaging capability of PDS imaging system for the surface object, we also took images of the moon surface. We used one pair of images as the input, at this time PDS degenerated into PD. As shown in Fig. 6, after PDS calutation, many details on the moon surface can be seen from the restored image and the resolution was increased obviously. And this proves that the PDS imaging system can detect the wave-front of extended object and get high resolution images.

5. Conclusions

In this paper, we built the PDS imaging system on a 1.23 m telescope, solve the image rotation problem between channels, and give the object function when the readout noise between channels is inconsistent. We made observation for different space objects by PDS imaging system and the results proved that PDS imaging system can restore the image correctly. We quantitatively tested the image restoration capability of PDS system and verified the restoration capability of PDS system for extended objects. Compared to the AO system, the cost of PDS system component and maintenance is very low, and it can get clear images for extended object. At present, the PDS imaging system designed in this paper had already been used in observation experiments on a 1.23 m telescope for a long time, so it will be the essential subsystem for one meter scale telescope. For the future work, we will try to observe the space objects in daytime on PDS imaging system and get the high resolution images.

Acknowledgements

The authors would like to thank Department of Electro-Optical Detection, Changchun Institute of Optics, Fine Mechanics and

Physics, Chinese Academy of Sciences, for providing raw images. The work was supported by the National High-Tech Research & Development Program of China (Grant No. 2008AA8080202).

References

[1] M.C. Roggemann, B.M. Welsh, Imaging Through Turbulence, CRC Press, Washington, DC, 1996.
[2] P.K. Shrestha, Y.T. Chun, D. Chu, A high-resolution optically addressed spatial light modulator based on ZnO nanoparticles, Light Sci. Appl. 4 (2015) e259.
[3] M.J. Booth, Adaptive optical microscopy: the ongoing quest for a perfect image, Light Sci. Appl. 3 (2014) e165.
[4] L. Chen, J. Lei, J. Romero, Quantum digital spiral imaging, Light Sci. Appl. 3 (2014) e153.
[5] T. Strudley, R. Bruck, B. Mills, et al., An ultrafast reconfigurable nanophotonic switch using wavefront shaping of light in a nonlinear nanomaterial, Light Sci. Appl. 3 (2014) e207.
[6] P. Girshovitz, N.T. Shaked, Doubling the field of view in off-axis low-coherence interferometric imaging, Light Sci. Appl. 3 (2014) e151.
[7] N. Caselli, F. Intonti, F.L. China, et al., Ultra-subwavelength phase-sensitive Fano-imaging of localized photonic modes, Light Sci. Appl. 4 (2015) e326.
[8] J.H. Seldin, R.G. Paxman, Phase-diverse speckle reconstruction of solar data. Image reconstruction and restoration, Proc. SPIE 2302 (1994) 268–280.
[9] Y.H. Wu, B. Wang, J.Y. Zhao, et al., Restoration of broadband white light image using phase diversity technique, Opt. Precision Eng. 18 (2010) 1849–1854 (in Chinese).
[10] R.G. Paxman, T.J. Schulz, J.R. Fienup, Joint estimation of object and aberrations by using phase diversity, J. Opt. Soc. Am. A: Opt. Image Sci. Vis. 9 (1992) 1072–1085.
[11] R.G. Paxman, J.H. Seldin, M.G. Löfdahl, et al., Evaluation of phase-diversity techniques for solar-image restoration, Astrophys. J. 466 (1996) 1087–1099.
[12] B.J. Thelen, R.G. Paxman, D.A. Carrara, et al., Maximum a posteriori estimation of fixed aberrations, dynamic aberrations, and the object from phase-diverse speckle data, J. Opt. Soc. Am. A: Opt. Image Sci. Vis. 16 (1999) 1759–1768.
[13] C.R. Vogel, Computational Methods for Inverse Problems, SIAM Press, Philadelphia, PA, 2002.
[14] C.R. Vogel, T. Chan, R. Plemmons, Fast algorithms for phase diversity-based blind deconvolution, adaptive optical system technologies, Kona, Hawaii, USA, SPIE 3353 (1998) 994–1005.
[15] M.G. Löfdahl, T.E. Berger, R.S. Shine, et al., Preparation of a dual wavelength sequence of high-resolution solar photospheric images using phase diversity, Astrophys. J. 495 (1998) 965–972.
[16] M.G. Löfdahl, G.B. Scharmer, Wave-front sensing and image restoration from focused and defocused solar images, Astron. Astrophys. 107 (1994) 243–264.
[17] B. Denolle, F. Cassaing, J. Montri, et al., Real-time focal-plane wavefront sensing for compact imaging phased-array telescopes: numerical and experimental demonstration Proc. SPIE, 8713, 2013, 87130J.
[18] A. Blanc, M. Mugnier, J. Idier, Marginal estimation of aberrations and image restoration by use of phase diversity, J. Opt. Soc. Am. A: Opt. Image Sci. Vis. 20 (2003) 1035–1045.
[19] J.L. Wang, Z.Y. Wang, B. Wang, et al., Image restoration by phase-diversity speckle, Opt. Precision Eng. 19 (2011) 1165–1170 (in Chinese).
[20] R.H. Byrd, P. Lu, J. Nocedal, et al., A limited memory algorithm for bound constrained optimization, in: Report NAM-08, EECS Department, Northwestern University, 1994.
[21] C. Zhu, R.H. Byrd, P. Lu, et al., LBFGS-B: Fortran subroutines for large-scale bound constrained optimization, in: Report NAM-11, EECS Department, Northwestern University, 1994.
[22] J.A. Parker, R.V. Kenyon, D.E. Troxel, Compare of interpolation methods of image resampling, IEEE Trans. Med. Imaging 22 (1983) 31–39.
[23] R. Kammel, R. Ackermann1, J. Thomas, et al, Enhancing precision in fs-laser material processing by simultaneous spatial and temporal focusing, Light Sci. Appl. 3 (2014) e169.
[24] B. Wang, Z.Y. Wang, J.L. Wang, et al., Phase-diverse speckle imaging with two cameras, Opt. Precision Eng. 19 (2011) 1384–1390 (in Chinese).
[25] J. Zhao, C. Zhan, B. Wang, et al., Parallelity improvement of object function for phase diversity, Opt. Precision Eng. 20 (2012) 431–438 (in Chinese).